ELSEVIER

Journal of Fluids and Structures 25 (2009) 1029–1048

JOURNAL OF FLUIDS AND STRUCTURES

www.elsevier.com/locate/jfs

Flow-induced oscillation of two circular cylinders in tandem arrangement at low Re

T.K. Prasanth, S. Mittal*

Department of Aerospace Engineering, Indian Institute of Technology, Kanpur, UP 208 016, India

Received 12 January 2008; accepted 4 April 2009
Available online 22 May 2009

Abstract

Results are presented for flow-induced vibrations of a pair of equal-sized circular cylinders of low nondimensional mass ($m^* = 10$) in a tandem arrangement. The cylinders are free to oscillate both in streamwise and transverse directions. The Reynolds number, based on the free-stream speed and the diameter of the cylinders, D is 100 and the centre-to-centre distance between the cylinders is $5.5D$. The computations are carried out for reduced velocities in the range $2 \leq U^* \leq 15$. The structural damping is set to zero for enabling maximum amplitudes of oscillation. A stabilized finite element method is utilized to carry out the computations in two dimensions. Even though the response of the upstream cylinder is found to be qualitatively similar to that of an isolated cylinder, the presence of a downstream cylinder is found to have significant effect on the behaviour of the upstream cylinder. The downstream cylinder undergoes very large amplitude of oscillations in both transverse and streamwise directions. The maximum amplitude of transverse response of the downstream cylinder is quite similar to that of a single cylinder at higher Re beyond the laminar regime. Lock-in and hysteresis are observed for both upstream and downstream cylinders. The downstream cylinder undergoes large amplitude oscillations even beyond the lock-in state. The phase between transverse oscillations and lift force suffers a 180° jump for both the cylinders almost in the middle of the synchronization regime. The phase between the transverse response of the two cylinders is also studied. Complex flow patterns are observed in the wake of the freely vibrating cylinders. Based on the phase difference and the flow patterns, the entire flow range is divided into five sub-regions.

Keywords: Vortex shedding; Two cylinders; Tandem arrangement; Vibration; Flow-induced; Finite element method

1. Introduction

A variety of engineering problems such as flow past heat exchanger tubes, chimney stacks, offshore structures and transmission lines involve vortex-induced vibration of multiple bluff bodies. The flow past a single oscillating cylinder has been studied by various researchers at both high and low Reynolds numbers. A comprehensive review of this flow problem can be found in the review articles by Williamson and Govardhan (2004), Sarpkaya (2004) and Bearman (1984). However, the flow around multiple vibrating cylinders has received much less attention. In the present work we address the free vibrations of two identical cylinders of diameter D in tandem arrangement in the laminar flow regime.

*Corresponding author. Tel.: +91 512 259 7906; fax: +91 512 259 7561.
E-mail address: smittal@iitk.ac.in (S. Mittal).

0889-9746/$ - see front matter © 2009 Elsevier Ltd. All rights reserved.
doi:10.1016/j.jfluidstructs.2009.04.001

Compared to a single cylinder the flow past two cylinders is much more complex. The additional geometric parameters in the form of the spacing between the cylinders add another dimension to the richness of the vortex dynamics. The change in spacing between the cylinders can very significantly affect the vortex shedding from both cylinders. Several experimental studies have been conducted in the past to understand the flow around two stationary cylinders in various arrangements. Zdravkovich (1977) classified the various possible arrangements in three categories based on the spacing and orientation of the cylinders to the flow direction. Proximity interference takes place when the cylinders are placed very close to each other. Wake interference occurs when the downstream cylinder is partly or fully submerged in the wake of the upstream cylinder. In the overlapping regime the effect of both proximity and wake interferences are combined. Mittal et al. (1997) carried out a computational study in two dimensions to investigate the interference effects in flows involving a pair of cylinders in tandem and staggered arrangements at $\mathrm{Re} = 100$ and 1000. They observed that the downstream cylinder, which lies in the wake of the upstream cylinder, experiences very large unsteady forces. Sumner et al. (2000) identified different flow patterns in the flow past two cylinders in staggered arrangement. For pitch ratios greater than $3D$–$4D$ and small angle of incidence, they observed that the Kármán vortices shed from the upstream cylinder impinge upon the downstream cylinder thereby disturbing the vortex shedding from the latter. Papaioannou et al. (2006) studied the flow around two stationary cylinders in tandem arrangement in the laminar and early turbulent regime ($\mathrm{Re} = 100-1000$) using two- and three-dimensional direct numerical simulations. The spacing between the cylinders was varied from $1.1D$ to $5.0D$. They observed that the critical spacing for vortex formation and shedding in the gap region depends on the Reynolds number. The exact value of critical spacing was found to be dependent on three-dimensionality.

When one or both cylinders are free to vibrate, the vortex shedding pattern of the two cylinders can undergo substantial modification. King and Johns (1976) studied the wake interaction of two flexible circular cylinders in water in tandem arrangements with a centre-to-centre gap of $0.25D$–$6D$. They used uncoupled and coupled cylinders with elastic/rigid members for the study. Depending on the centre-to-centre gap and reduced velocity, three modes of vibration were observed: the fundamental mode in-line, the second normal mode in-line and fundamental mode cross-flow. Based on a detailed investigation of flow-induced oscillations of two cylinders in various arrangements, Zdravkovich (1985) found that the oscillations of the cylinders depend very strongly on their relative locations. Their response could be classified into three categories where (i) instability makes the amplitude build up rapidly to extremely large values, predominantly in the streamwise direction; (ii) instability makes the amplitude slowly build up to a certain level in the streamwise direction; (iii) instability makes the amplitude gradually build up to large values predominantly in the transverse direction. Bokaian and Geeola (1984a, b) studied the fluid-dynamic instability of a circular cylinder free to oscillate only in the transverse direction in the wake from an identical stationary body. They reported that depending on the cylinder separation and structural damping, the cylinder exhibited a vortex-resonance, or a galloping or a combined vortex-resonance and galloping or a separated vortex-resonance and galloping behaviour.

Mahir and Rockwell (1996a, b) studied the vortex formation in the flow around two oscillating cylinders in tandem arrangement at $\mathrm{Re} = 160$. The cylinder system was subjected to controlled excitation over a range of frequencies and phase angles between the oscillating cylinders. They observed that two cylinders subjected to forced oscillation can generate locked-in patterns of vortices over a range of excitation frequencies. When the separation was large, the frequency range of lock-in was similar to that for a single cylinder. Laneville and Brika (1999) investigated the effect of mechanical coupling of two cylinders in tandem arrangement. They observed that when the cylinders were coupled only by fluid, the upstream one behaved like an isolated cylinder. The response of the downstream cylinder, on the other hand, varied with spacing between the cylinders. The response of both the cylinders were found to be hysteretic in nature. Mittal and Kumar (2001) studied free vibrations of two equal-sized cylinders in both tandem and staggered arrangements for $\mathrm{Re} = 100$. The cylinders were separated by a distance of 5.5 times the diameter in the streamwise direction. Computations were carried out for three values of nondimensional structural frequency, F_N, that were either close to or equal to the vortex shedding frequency for the stationary cylinders. In all the cases studied, the upstream cylinder was found to behave like a single cylinder. The downstream cylinder, lying in the wake of the upstream one, was found to experience wake-induced flutter. The term wake-induced flutter derives its name from its resemblance to classical flutter of airplane wings involving motions in two or more degrees of freedom. A similar study was later conducted for the $\mathrm{Re} = 1000$ flow (Mittal and Kumar, 2004). The present study is a comprehensive analysis of VIV of two cylinders for a range of reduced velocities ($2 < U^* < 15$). It addresses various important phenomena like synchronization, hysteresis, phase difference between lift force and transverse oscillation and between the transverse oscillations of two cylinders. It also attempts to classify the U^* regime with respect to phase-difference variation and flow patterns.

Jester and Kallinderis (2004) carried out a numerical study for forced and free transverse vibrations of a pair of cylinders in tandem and side-by-side arrangements for $\mathrm{Re} = 1000$. They observed a wake-galloping effect; the downstream cylinder, in the wake of the upstream cylinder, undergoes large amplitude free vibration over a wide range of flow velocities. They also observed a secondary peak in the variation of amplitude for rigidly connected cylinders in

tandem arrangement undergoing free vibrations. Assi et al. (2006) experimentally studied the interference between two cylinders (Re = 3000–13 000). The upstream cylinder was fixed while the downstream one was mounted on elastic supports and allowed to oscillate only transversely to the flow direction. Interference galloping was observed for centre-to-centre of $2D$–$5.6D$ between the cylinders where a continuous increase in the response of the cylinder is observed with increasing reduced velocity. Carmo et al. (2007) in their study of flow-induced vibration of two cylinders in tandem arrangement reported large amplitude of oscillation of the downstream cylinder. The upstream cylinder was fixed and the downstream cylinder with $m^* = 2$ was free to oscillate only transverse to the flow. The centre-to-centre distance was varied from $3D$ to $8D$ and the computations were carried out at Re = 150 by varying the reduced velocity. Interestingly, their results did not show wake-galloping. The r.m.s value of the lift coefficient observed for the downstream cylinder was very large compared to the isolated cylinder. Papaioannou et al. (2008) studied the effect of spacing on the vortex-induced vibrations of two tandem cylinders numerically. The computations were carried out in two dimensions for cylinder spacing in the range $2.5D$–$5D$ at a fixed Reynolds number, Re = 160. The cylinders were free to oscillate in both in-line and transverse directions. The cylinder spacing was found to affect the response of the cylinders in a number of ways. The range as well as onset of synchronization was found to vary with cylinder spacing along with the maximum amplitude of oscillation of the downstream cylinder. The hysteresis effect and upper branch, known to exist for a single oscillating cylinder, were not observed in their study. This was attributed to the mass-damping parameter, Reynolds number and two-dimensional calculations.

In this paper, we investigate the free vibrations of two identical cylinders in tandem arrangement in the laminar flow regime. The Reynolds number, based on the diameter of the cylinders, is 100. The cylinders are free to vibrate in both in-line and transverse flow directions. The centre-to-centre spacing between the two cylinders is $5.5D$. The details of the flow past stationary cylinders in this configuration can be found in an earlier work by us (Mittal et al., 1997). This spacing is sufficient for the upstream cylinder to experience independent vortex shedding. The downstream cylinder lies in the unsteady wake of the upstream cylinder leading to wake interference. Some of the questions that we address in this work are: (a) How different is the response of the two cylinders compared to that of a single cylinder? (b) What kind of flow patterns, even at this low enough Re should one expect? (c) As in the case of single cylinder, does the flow and cylinder response exhibit hysteresis? (d) What is the behaviour of the phase between the lift and transverse response of the cylinders? (e) What is the phase between the response of the upstream and downstream cylinders and its relevance in the context of flow patterns?

The outline of the rest of the article is as follows. A brief review of the governing equations for incompressible fluid flow and the motion of a rigid body under the influence of unsteady fluid forces is given in Section 2. The stabilized space–time finite element formulation utilized to solve the governing equations is given in Section 3. Section 4 describes the problem set-up, initial and boundary conditions used and the mesh moving scheme along with a mesh resolution study. Results for free vibrations of the two cylinder system and comparison with the results of the free vibrations in the flow around a single cylinder, obtained in a previous work by Singh and Mittal (2005), are presented in Section 5. We finish with a few concluding remarks in Section 6.

2. The governing equations

2.1. The incompressible flow equations

Let $\Omega_t \subset \mathbb{R}^{n_{sd}}$ and $(0, T)$ be the spatial and temporal domains, respectively, where n_{sd} is the number of space dimensions, and let Γ_t denote the boundary of Ω_t. The spatial and temporal coordinates are denoted by $\mathbf{x}$ and t. The Navier–Stokes equations governing incompressible fluid flow are

$$\rho\left(\frac{\partial \mathbf{u}}{\partial t} + \mathbf{u}\cdot\nabla\mathbf{u} - \mathbf{f}\right) - \nabla\cdot\boldsymbol{\sigma} = 0 \quad \text{on } \Omega_t \times (0,T), \tag{1}$$

$$\nabla\cdot\mathbf{u} = 0 \quad \text{on } \Omega_t \times (0,T). \tag{2}$$

Here ρ, $\mathbf{u}$, $\mathbf{f}$ and $\boldsymbol{\sigma}$ are the density, velocity, body force and the stress tensor, respectively. The stress tensor is written as the sum of its isotropic and deviatoric parts:

$$\boldsymbol{\sigma} = -p\mathbf{I} + \mathbf{T}, \quad \mathbf{T} = 2\mu\boldsymbol{\varepsilon}(\mathbf{u}), \quad \boldsymbol{\varepsilon}(\mathbf{u}) = \tfrac{1}{2}((\nabla\mathbf{u}) + (\nabla\mathbf{u})^{\mathrm{T}}), \tag{3}$$

where p and μ are the pressure and dynamic viscosity, respectively. Both the Dirichlet and Neumann-type boundary conditions are accounted for, represented as

$$\mathbf{u} = \mathbf{g} \quad \text{on } (\Gamma_t)_g, \quad \mathsf{n}\cdot\boldsymbol{\sigma} = \mathbf{h} \quad \text{on } (\Gamma_t)_h, \tag{4}$$

where $(\Gamma_t)_g$ and $(\Gamma_t)_h$ are complementary subsets of the boundary Γ_t and n is its unit normal vector. The details of the boundary conditions for the present problem are shown in Fig. 1 and given in Section 4.1. For the freely vibrating cylinder the velocity of the fluid on the cylinder surface is determined by solving the equation of motion for the spring mounted oscillator. The initial condition on the velocity is specified on Ω_t at $t = 0$:

$$\mathbf{u}(\mathbf{x}, 0) = \mathbf{u}_0 \quad \text{on } \Omega_0, \tag{5}$$

where $\mathbf{u}_0$ is divergence free.

2.2. The equations of motion for a rigid body

A solid body immersed in the fluid experiences unsteady forces and in certain cases may exhibit rigid body motion. The motion of the body, in the two directions along the Cartesian axes, is governed by the following equations:

$$\ddot{X} + 4\pi F_N \zeta \dot{X} + (2\pi F_N)^2 X = \frac{2C_D}{\pi m^*} \quad \text{for } (0, T), \tag{6}$$

$$\ddot{Y} + 4\pi F_N \zeta \dot{Y} + (2\pi F_N)^2 Y = \frac{2C_L}{\pi m^*} \quad \text{for } (0, T). \tag{7}$$

Here, F_N is the reduced natural frequency of the oscillator, ζ the structural damping ratio, m^* the nondimensional mass of the body while C_L and C_D are the instantaneous lift and drag coefficients for the body, respectively. The free-stream flow is assumed to be along the x-axis. $\ddot{X}$, $\dot{X}$ and X denote the normalized in-line acceleration, velocity and displacement of the body, respectively, while $\ddot{Y}$, $\dot{Y}$ and Y represent the same quantities associated with the cross-flow motion. In the present study, in which the rigid body is a circular cylinder, the displacement and velocity are normalized by the diameter, D, of the cylinder and the free-stream speed, U, respectively. The reduced natural frequency of the system, F_N is defined as $f_N D/U$ where f_N is the natural frequency of the oscillator. Another related parameter is the reduced velocity, U^*. It is defined as $U^* = U/f_N D = 1/F_N$. The nondimensional mass of the cylinder is defined as $m^* = 4m/\pi\rho D^2$, where m is the actual mass of the oscillator per unit length and ρ is the density of the fluid. The equations governing the fluid flow are solved in conjunction with those for the motion of each of the two cylinders. The force coefficients are computed by carrying out an integration of the pressure and viscous stresses around the circumference of the cylinder:

$$C_D = \frac{1}{\frac{1}{2}\rho U^2 D} \int_{\Gamma_{\text{cyl}}} (\boldsymbol{\sigma}\mathsf{n}) \cdot \mathsf{n}_\mathsf{x} \, d\Gamma, \quad C_L = \frac{1}{\frac{1}{2}\rho U^2 D} \int_{\Gamma_{\text{cyl}}} (\boldsymbol{\sigma}\mathsf{n}) \cdot \mathsf{n}_\mathsf{y} \, d\Gamma. \tag{8,9}$$

Here n_x and n_y are the Cartesian components of the unit vector n that is normal to the cylinder boundary Γ_{cyl}. These coefficients include the fluid dynamic damping and the added mass effect. The resulting drag and lift coefficients are used to compute the displacement and velocity of the body via Eqs. (6) and (7). This information is then used to update the location of the body and the no-slip boundary condition for the velocity field on the body surface.

3. The finite element formulation

To accommodate the motion of the cylinder and the deformation of the mesh, the deforming spatial domain/stabilized space–time (DSD/SST) method proposed by Tezduyar et al. (1992a, b) is utilized. Equal-in-order basis functions for velocity and pressure, that are bilinear in space and linear in time, are used. Details of the formulation including those of the stabilization coefficients and its implementation for oscillating cylinders can be found in articles by Tezduyar et al. (1992a–c), Mittal (1992), Mittal and Kumar (2001) and Singh and Mittal (2005). The time integration of the oscillator equation is done using the space–time method given in Mittal (1992).

4. Problem description

Two cylinders, each of diameter D and mass ratio $m^* = 10$, are mounted on elastic supports in a tandem arrangement. The centre-to-centre spacing between the two cylinders is $5.5D$. For this arrangement the downstream cylinder is expected to lie in the unsteady wake of the upstream one. They are free to vibrate both in the streamwise and transverse directions. To encourage high amplitude oscillations, the structural damping coefficient is set to zero. The springs in both the in-line and transverse directions are assumed to be linear and have the same stiffness. Singh and

Mittal (2005) studied the relative effect of Re and U^* on the response of a single cylinder undergoing vortex-induced vibration. Two sets of computations were carried out. In the first set of computations Re was set to 100 and the reduced velocity, U^*, was varied. In the second set of computations the reduced velocity was fixed at $U^* = 4.92$ while the Reynolds number was varied. Both sets of computations showed similar behaviour. In this study the Reynolds number is fixed ($Re = 100$) and U^* is varied by varying the natural frequency of the oscillator. The Reynolds number, Re, is based on the freestream speed, U, diameter of the cylinder, D, and viscosity of the fluid.

It has been shown that the blockage has a very significant effect on the bluff body flows (Prasanth et al., 2006; Prasanth and Mittal, 2008; Mittal et al., 2006). In particular, for $m^* = 10$ and Re near 100 it was shown by Prasanth and Mittal (2008) that a blockage of more than 2.5% can lead to a hysteretic behaviour of the cylinder response and flow field at the onset of synchronization for a freely vibrating cylinder. Compared to an unbounded flow, a higher blockage also leads to incorrect prediction of aerodynamic forces. Therefore, for this study, the lateral boundaries were placed $25D$ from the cylinder centre, resulting in a blockage of 2%. The upstream and downstream boundaries are placed at $25D$ and $105.5D$ from the centre of the upstream cylinder, respectively.

4.1. Boundary conditions

No-slip condition is applied for the velocity at the surface of the two cylinders. The flow velocity of each of the two cylinders and their locations are updated at each nonlinear iteration by solving the equations of motion for each oscillator. As can be seen in Fig. 1, the outer boundary of the computational domain is a rectangle. Freestream values are assigned for the velocity at the upstream boundary and the viscous stress vector is set to zero at the downstream boundary. On the upper and lower boundaries, the component of the velocity normal to the boundary and the component of the stress vector along these boundaries are prescribed zero. The boundary conditions are also shown in Fig. 1.

4.2. Finite element mesh and mesh moving scheme

A close-up view of the finite element mesh used for the computation is shown in Fig. 2. The mesh consists of 40 197 nodes and 39 648 quadrilateral, four noded elements. Each cylinder resides in a square box. The structured mesh inside the box is made of radial and circumferential grid lines. The circumferential lines are circular close to the cylinder and gradually straighten out to fit the box as one moves out radially. The element size increases nonuniformly in the radial direction within this box. The thickness of the first layer of elements on the cylinder boundary in the radial direction is

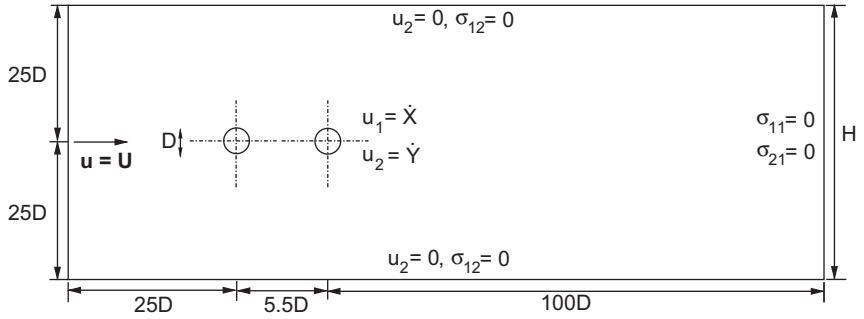

Fig. 1. Flow past two cylinders in tandem: schematic of the computational domain. The boundary conditions are marked as well.

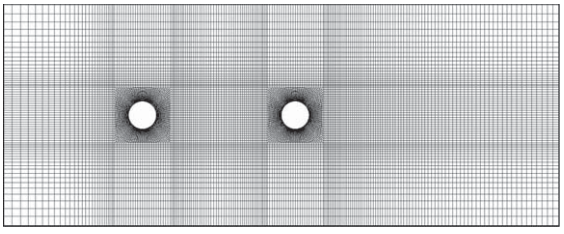

Fig. 2. Flow past two cylinders in tandem: a close up view of the finite element mesh.

Table 1
Re = 100, $U^* = 5.5$ flow past freely vibrating cylinders in tandem: effect of mesh resolution on various quantities.

Mesh	Nodes	Elements	Cylinder	$Y_{\max}/D$	Y_{rms}/D	X_{rms}/D	$C_{L_{\max}}$	$C_{D_{\mathrm{rms}}}$
M20k	23897	23472	Upstream	0.6113	0.4325	0.0171	0.6021	0.2793
			Downstream	0.2619	0.1851	0.002745	0.2413	0.0448
M40k	40195	39648	Upstream	0.6087	0.4304	0.0171	0.6033	0.2853
			Downstream	0.2630	0.1859	0.002688	0.2421	0.0451
M80k	80085	79272	Upstream	0.6045	0.4285	0.0169	0.6155	0.2823
			Downstream	0.2710	0.1916	0.002756	0.2501	0.0465

$0.0125D$. It is $0.0325D$ in the tangential direction. The mesh moving scheme has been designed such that the mesh in the square box around the cylinder moves along with the cylinder as a rigid body. The location of the outer boundary is fixed. As a result, the movement of the cylinder causes deformation of the mesh points lying between the two squares and the outer boundary. This kind of mesh movement is very inexpensive, retains the connectivity of the nodes and is expected to lead to almost no projection errors in the near wake of the cylinders, as shown in Mittal (1992) and Mittal and Tezduyar (1992).

4.2.1. Mesh resolution and time-step study

Computations were carried out on three meshes to investigate the adequacy of the mesh being used. The details of the meshes are given in Table 1. Compared to the mesh M20k, the extra grid points in meshes M40k and M80k, were mostly distributed in the regions close to and in between the two cylinders. Computations were carried out for $U^* = 5.5$. For this value of reduced speed both upstream and downstream cylinders undergo fairly large transverse oscillations. The initial condition for the computations was the fully developed unsteady flow past stationary cylinders. The nondimensional time step used was $\Delta t = 0.05$. A summary of the results, for the fully developed flow, obtained with the three meshes is presented in Table 1.

From Table 1 it is seen that the values obtained with the three meshes are within 5% of each other. In addition, the results from mesh M40k are very close to the ones from the more refined mesh, M80k. Amongst all the quantities, the maximum lift coefficient appears to be the most sensitive. The difference in the values for $C_{L_{\max}}$, from the two meshes, for the upstream cylinder is, approximately, 2% for the upstream and 3% for the downstream cylinder. This establishes the adequacy of mesh M40k in computing the free vibrations of two cylinders. All the results in this paper have been computed using the M40k mesh.

Table 2 shows the effect of time step ($\Delta t = 0.025$ and 0.005) on various quantities. Amongst all quantities the maximum variation observed is for the r.m.s value of the drag coefficient of the downstream cylinder. The difference in this value from the two values of Δt is less than 2.4%. The difference in other quantities is much less. These results can also be compared with the ones obtained with $\Delta t = 0.05$ and shown in Table 1. Barring the exception of the r.m.s value of the drag coefficient the results for $\Delta t = 0.05$ are within 2.2% of the ones obtained with $\Delta t = 0.005$. For example, the difference in the amplitude of transverse response is less than 1%. Therefore, $\Delta t = 0.05$ is utilized for further computations.

5. Results: free vibration of two cylinders in tandem

5.1. Frequency of oscillation and synchronization/lock-in

One of the most significant effects of vibration of the cylinder on its wake is synchronization or lock-in where the vortex shedding frequency undergoes a drastic change from that of a stationary cylinder to a value close to the natural frequency of the system. Fig. 3 shows the variation of the nondimensional transverse oscillation frequency of upstream and downstream cylinders in tandem with U^*. The variation of the reduced natural frequency of the system, F_N, and nondimensional transverse oscillation frequency for a single cylinder are also shown. At $U^* = 3.0$ the normalized vortex shedding frequency of both cylinders in tandem arrangement is found to be 0.1523. This is very close to the vortex shedding frequency from stationary cylinders (= 0.1503). Sumner et al. (2000) also found that the Strouhal numbers corresponding to the measurements in the wakes of upstream and downstream cylinders in staggered arrangement have

Table 2
Re = 100, $U^* = 5.5$ flow past freely vibrating cylinders in tandem: effect of time-step on various quantities.

Δt	Cylinder	Y_{max}/D	Y_{rms}/D	X_{rms}/D	$C_{L_{max}}$	$C_{D_{rms}}$
0.025	Upstream	0.6092	0.4331	0.01707	0.5923	0.2742
	Downstream	0.2616	0.1851	0.002635	0.2415	0.0438
0.005	Upstream	0.6089	0.4307	0.0170	0.5899	0.2709
	Downstream	0.2604	0.1850	0.002631	0.2461	0.0428

The mesh utilized for the study is M40k.

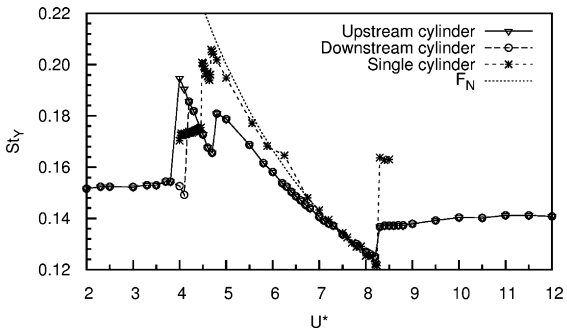

Fig. 3. Re = 100 flow past freely vibrating cylinders in tandem: variation of nondimensional transverse oscillation frequencies (St_Y) of the two cylinders along with that for single cylinder presented in Singh and Mittal (2005).

the same value. They attributed this to the synchronization between the impingement of flow and Kármán vortex shedding from the downstream cylinder.

Synchronization or lock-in is observed for a range of U^* for both upstream and downstream cylinders as seen in Fig. 3. Near the onset of lock-in the jump in vortex shedding frequency occurs in two steps. In the first step ($U^* \sim 4$) the jump occurs to a frequency which is in between the vortex shedding frequency of the stationary cylinder and natural frequency of the system. Both the cylinders undergo a soft lock-in before the primary lock-in. During soft lock-in the vortex shedding frequency is different from the natural frequency of the system. It is found to vary almost linearly with U^* for a small range of U^*. This is similar to the observation made by Mittal and Kumar (1999), Singh and Mittal (2005) and Prasanth et al. (2006) for a single cylinder of low m^* undergoing free-vibrations. The range of U^* for which the upstream and downstream cylinders undergo soft lock-in is much larger than that for a single cylinder. This is followed by another jump which takes the vortex shedding frequency close to the natural frequency of the system. Except for a small range of U^* at the onset of lock-in, the transverse oscillation frequency of upstream cylinder and downstream cylinders are found to be identical for the remaining values of U^*. This is in-line with the observation of Mittal and Kumar (2001) where the nondimensional frequencies of time variation of lift coefficient and cross-flow oscillations of both cylinders were found equal. At $U^* = 8.3$ the vortex shedding frequency jumps to a value which is higher than the natural frequency of the system. It remains almost constant for all higher values of U^*. This marks the end of synchronization for both upstream and downstream cylinders. It is interesting to note that outside the lock-in range, the nondimensional transverse oscillation frequency for both cylinders in tandem is less than that for a single cylinder. This indicates that the presence of an oscillating downstream cylinder has a considerable influence on the vortex shedding of the upstream cylinder despite a centre-to-centre streamwise spacing of $5.5D$.

5.2. Response of the cylinders

Fig. 4 shows the variation of the nondimensional maximum amplitude of the transverse displacement of the upstream and downstream cylinders with U^*. The corresponding variation for a single cylinder, presented in Singh and Mittal (2005), is also shown in the figure. Also shown are the Lissajous figures for the in-line and transverse displacements of the two cylinders for the fully developed flows at various U^*. The maximum amplitude that is being reported is the peak value of the response beyond the initial transience and after a fully developed state has been achieved. In general, the response of the upstream cylinder is qualitatively similar to the response of the single cylinder. The maximum amplitude

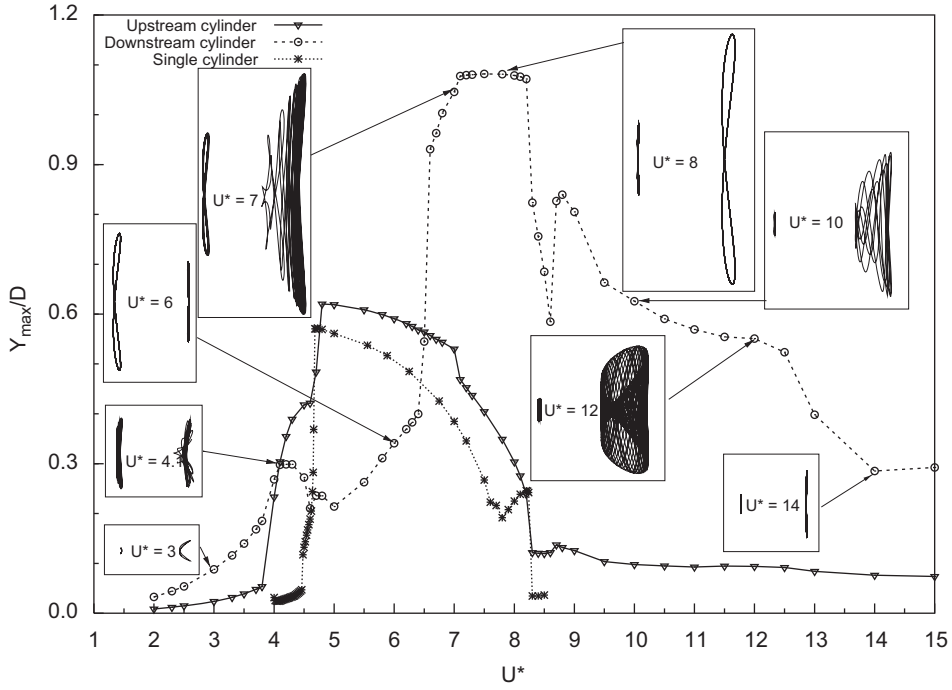

Fig. 4. Re = 100 flow past freely vibrating cylinders in tandem: variation of the maximum amplitude of the transverse oscillation with U^* for the two cylinders. For reference, the response of a single cylinder presented in Singh and Mittal (2005) is also shown. The Lissajous figures for the trajectory of the centre of the cylinders are shown at various U^*. For enhancing clarity, the longitudinal spacing between the Lissajous figures for upstream and downstream cylinders has been reduced and the figures have been amplified.

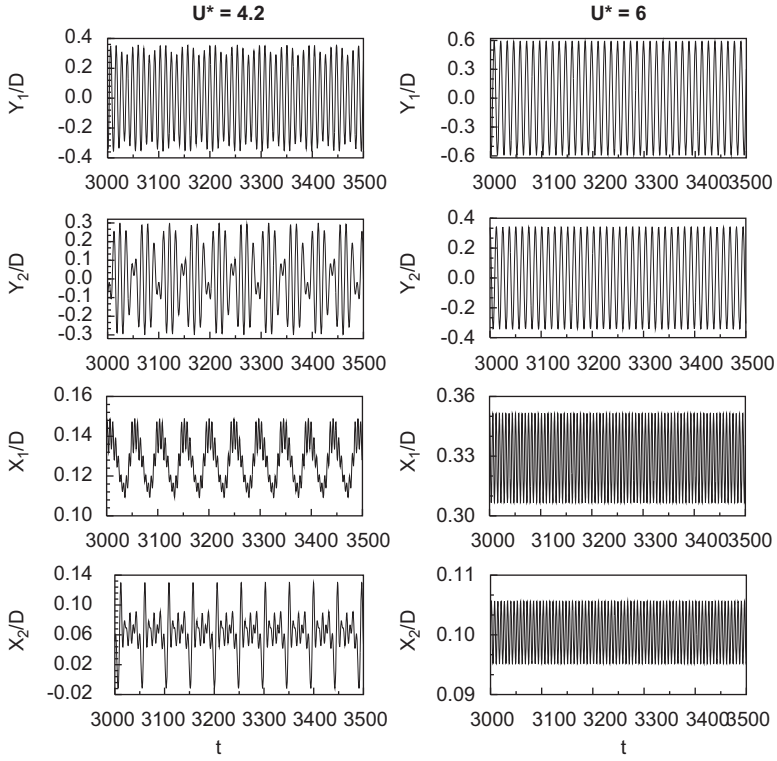

Fig. 5. Re = 100 flow past freely vibrating cylinders in tandem: time histories of transverse and in-line oscillations of both upstream (subscript 1) and downstream (subscript 2) cylinders at $U^* = 4.2$ (left) and $U^* = 6$ (right).

of oscillation is observed at almost the same reduced velocity, U^*. However, the presence of the downstream cylinder has some effect on the upstream one. For example, the oscillation amplitude of the upstream cylinder is higher than that of a single cylinder and the upstream cylinder shows large amplitude oscillations at lower U^* when compared to a single cylinder. For example, it can be seen from Fig. 4 that at $U^* = 4.5$ the upstream cylinder undergoes large amplitude oscillations, while the single cylinder suffers oscillations of much lower amplitude.

The transverse response of the downstream cylinder is found to be very different from that of the upstream cylinder. The maximum amplitude of transverse oscillations is very high ($\sim 1.1D$); it is almost twice the value for the upstream cylinder. From Fig. 4 it can be seen that, compared to the upstream cylinder, the downstream cylinder achieves its maximum amplitude at a larger U^* (~ 7.1) and retains it for a significant range of reduced speed, until the end of the synchronization regime (~ 8.3). Two additional peaks of the amplitude of transverse oscillations of the downstream cylinder are observed. The peak at $U^* \sim 4.2$ is related to the onset of synchronization. The other one, at $U^* \sim 8.8$, is related to the increased unsteadiness in the wake. Except for $4.2 < U^* < 6.6$ the downstream cylinder exhibits larger amplitude response compared to the upstream cylinder. Fig. 5 shows the time histories of transverse and in-line response of both upstream and downstream cylinders at $U^* = 4.2$ and 6 for the fully developed solution. A minimum of 200 vortex shedding cycles are computed after the system reaches a dynamic steady state; $U^* = 4.2$ is close to the onset of synchronization, while $U^* = 6$ lies within the synchronization regime. At $U^* = 4.2$, the upstream cylinder undergoes larger amplitude of oscillations compared to the downstream one. Beats are observed in the time histories of both transverse and in-line response of the cylinders. Steady periodic oscillations are observed from the time histories of the response of the cylinders at $U^* = 6$. This is typical of the response seen at other values of U^* in the synchronization regime. Time periodicity of the response is also seen in the Lissajous figures shown in Fig. 4.

Fig. 6 shows the response of a single cylinder undergoing free transverse vibrations from the experiments of Khalak and Williamson (1999) at much higher Reynolds number along with the results from the present study. The free vibrations of an isolated cylinder in the laminar regime show only the initial and lower branch. At high Re, beyond the laminar regime, there also exists the upper branch which is associated with larger amplitude of response of the cylinder. In Fig. 6 the maximum transverse oscillation amplitude is plotted against $U^*\mathrm{St}_0$, instead of $(U^*/f^*)\mathrm{St}_0$ as in Khalak and Williamson (1999). Here, St_0 is the Strouhal number corresponding to the vortex shedding frequency for flow past a stationary cylinder. The parameter $f^* = f/f_N$ is dropped because of the large difference in its value for low vs. high Re. The similarity between the data from the present laminar computations and data from Khalak and Williamson (1999) at much higher Re can be seen in this plot. However, there are some differences as well. The peak oscillation amplitude is observed near the end of lock-in regime for the present case, while for the single cylinder at higher Re it is observed on the upper branch near the lower U^* end of the lock-in range.

Fig. 7 shows a comparison of the present results for the maximum transverse displacement of the downstream cylinder with that from the previous studies. It is to be noted that the experimental parameters used in the various studies shown in Fig. 7 differ from each other. The parameters that can lead to difference in the response of the downstream cylinder are the Reynolds number, mass ratio, mass-damping parameter and centre-to-centre spacing of the cylinders. The cylinders in King and Johns (1976) were flexible in nature and the experiment was conducted at $1 \times 10^3 < \mathrm{Re} < 2 \times 10^4$. In the work of Assi et al. (2006) the upstream cylinder was stationary and Reynolds number was varied from 3×10^3 to 1.3×10^4. In all the cases shown in Fig. 7 the centre-to-centre spacing of the cylinders is $5D$ or higher which makes the comparison meaningful. Compared to the wake-galloping behaviour reported in King and Johns (1976) and Assi et al. (2006) where the maximum displacement of the cylinder increases smoothly with increase in U^*, the maximum transverse displacement in the present study occurs only for a range of U^*. From Fig. 7 it can be noted that the wake galloping has not been observed in all studies, especially in the lower Re regime. The result of Jester and Kallinderis (2004) ($\mathrm{Re} = 1000$) shows low amplitudes of oscillation at higher U^*. Carmo et al. (2007) reported the absence of wake-galloping behaviour at $\mathrm{Re} = 150$ with a centre-to-centre spacing of $3D$. Papaioannou et al. (2008) observed a similar response at $\mathrm{Re} = 160$ with a centre-to-centre spacing of $5D$. In their study, the maximum transverse oscillation amplitude of the downstream cylinder was found to decrease with increase in U^* after reaching a peak value. This shows that the Reynolds number plays an important role in the occurrence of wake-galloping behaviour.

Fig. 8(a) shows the variation of maximum value of the in-line displacement after subtracting the mean value for the two cylinders with U^*. Compared to the upstream cylinder, the downstream cylinder shows larger variation in the in-line response with U^*. The peak in the maximum value of the in-line amplitude for the downstream cylinder for $U^* \sim 3$ is attributed to the synchronization with the frequency of time variation of drag. It is well known that the drag oscillates with twice the frequency of the time variation of lift. The second peak in the in-line response (at $U^* \sim 4.2$) is coincident with the onset of synchronization. The third peak is observed at $U^* \sim 6.6$ when the natural frequency of the system is approximately equal to the vortex shedding frequency. This is followed by two sub-harmonic peaks: the first one at $U^* \sim 9$ and a second one at ~ 12. The variation of the mean in-line response of the two cylinders with respect to their

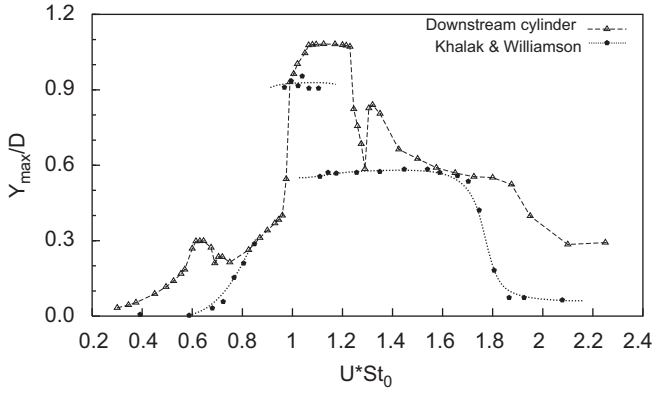

Fig. 6. Re = 100 flow past freely vibrating cylinders in tandem: variation of maximum transverse oscillation amplitude of the downstream cylinder. The present results (in solid line) are compared with that of a single cylinder at higher Re from Khalak and Williamson (1999) (in broken line). Here, St_0 is the Strouhal number corresponding to the vortex shedding frequency for flow past a stationary cylinder.

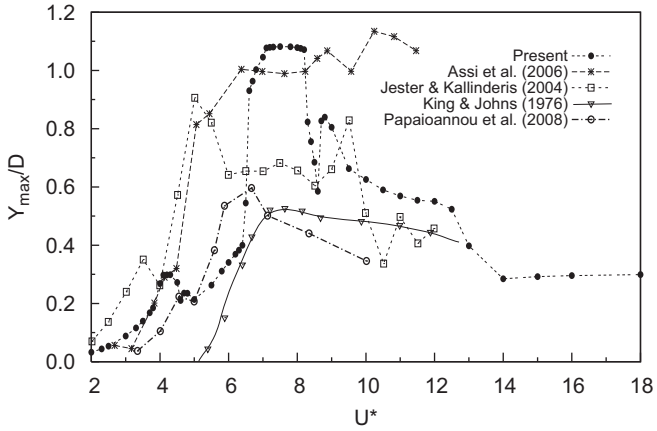

Fig. 7. A comparison of the results from literature with the variation of maximum transverse amplitude of oscillation of the downstream cylinder with U^* from the present study.

relative centres is shown in Fig. 8(b). Even though the average separation between the cylinders shows some variation with U^* the downstream cylinder lies in the wake interference regime for all U^* that have been studied.

5.3. Aerodynamic coefficients

Fig. 9(a) shows the variation of maximum lift coefficient on both upstream and downstream cylinders with U^*. For reference, the variation of maximum lift coefficient for an isolated cylinder presented in Singh and Mittal (2005) is also shown in the figure. The variation of maximum lift coefficient of the upstream cylinder is qualitatively similar to that of a single cylinder, except for an additional peak at $U^* \sim 4.5$ in the result of the upstream cylinder. However, the downstream cylinder results are different. The downstream cylinder is found to have a higher value of the lift coefficient compared to that of the upstream cylinder for $U^* \sim 2$–4. This is related to the modification of the vorticity distribution on the downstream cylinder owing to the impingement of vortices from the upstream cylinder. This can be seen from Fig. 10 which shows the variation of coefficient of pressure and vorticity on the surface of the two cylinders at time instants corresponding to the maximum lift coefficient. For both upstream and downstream cylinders, the maximum value of lift coefficient occurs at a much lower value of U^* than the one at which maximum transverse displacements occur. The peak lift coefficient experienced by the downstream cylinder is slightly larger than the upstream one and occurs at a lower U^*. As expected, the lift experienced by the cylinders begins to drop with U^* at the onset of lock-in.

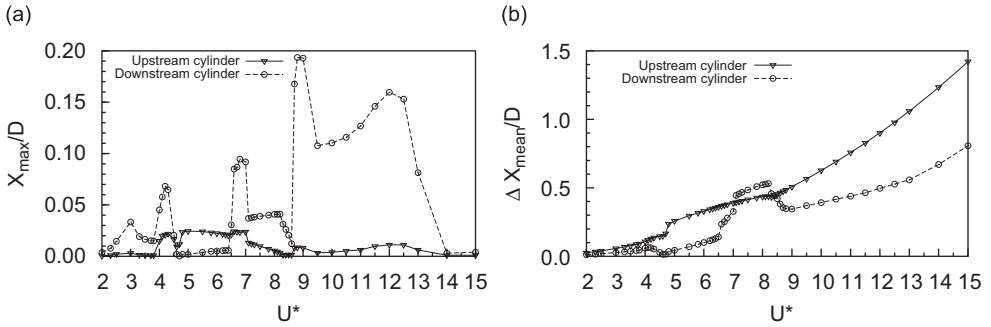

Fig. 8. Re = 100 flow past freely vibrating cylinders in tandem: variation of the (a) maximum value of the in-line displacement after subtracting the mean value and (b) mean value of in-line displacement of the upstream and downstream cylinders with U^*. The mean value shown is with respect to the cylinder centre.

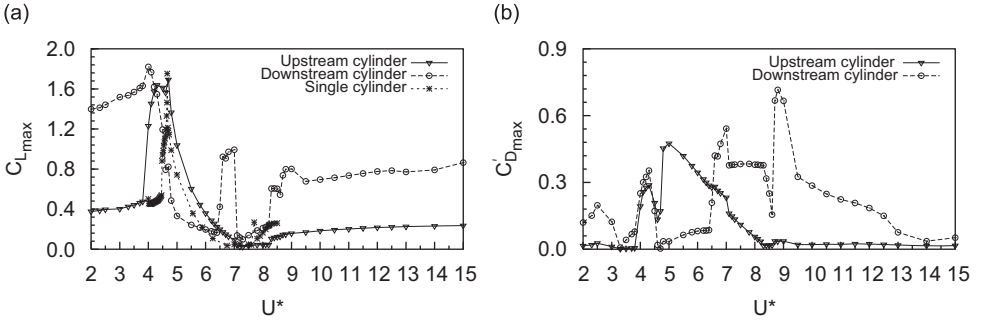

Fig. 9. Re = 100 flow past freely vibrating cylinders in tandem: variation of the maximum value of (a) lift coefficient and (b) drag coefficient with U^*. The corresponding variation for a single cylinder is also shown for comparison.

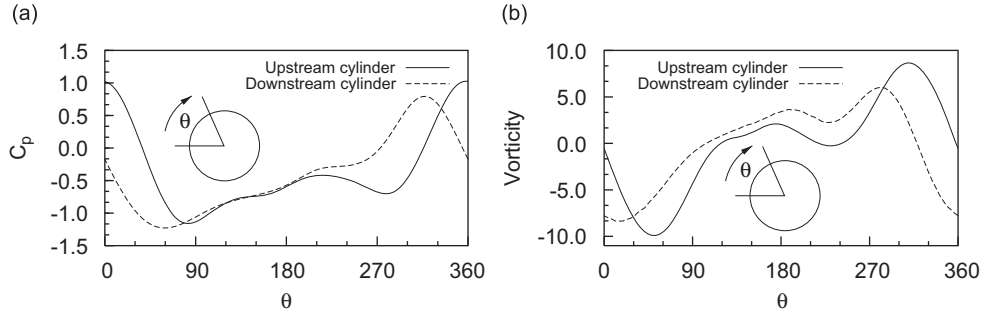

Fig. 10. Re = 100, $U^* = 3.3$ flow past freely vibrating cylinders in tandem: variation of (a) coefficient of pressure and (b) vorticity on the surface of the upstream and downstream cylinders. The plots correspond to the location of maximum lift coefficient for both cylinders.

For $4.3 < U^* < 6.3$, the maximum value of lift coefficient experienced by the downstream cylinder is smaller than that of the upstream cylinder and also than that of an isolated cylinder.

Fig. 9(b) shows the variation of the maximum value of drag coefficient, after subtracting the mean value, for both upstream and downstream cylinders with U^*. The variation of the maximum value of the drag coefficient of the upstream cylinder shows an additional local peak at $U^* \sim 4.5$. The variation for the downstream cylinder is different and presents a larger number of local peaks. The downstream cylinder experiences more drag compared to the upstream cylinder except for $4.5 < U^* < 6.6$. The time histories of lift and drag coefficients at $U^* = 4.2$ and 6 are shown in Fig. 11.

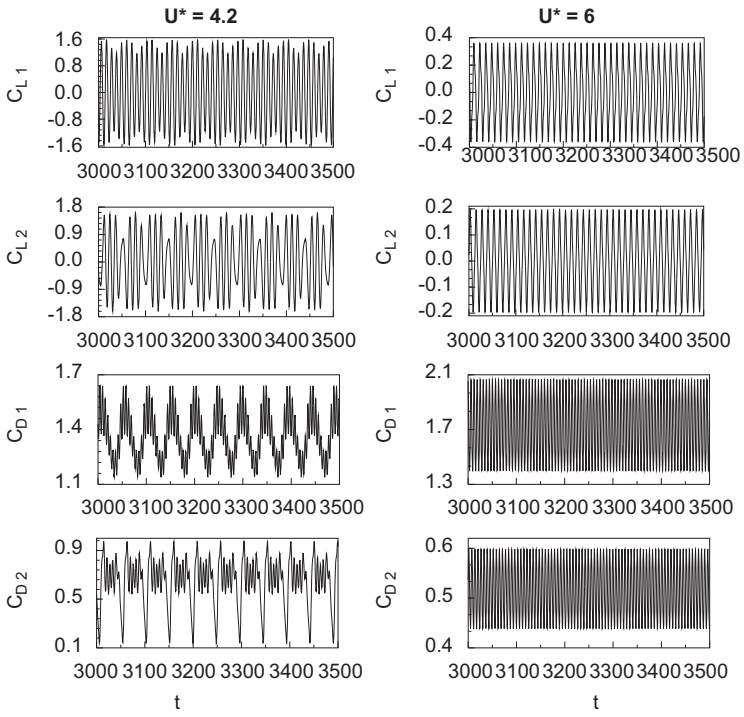

Fig. 11. Re = 100 flow past freely vibrating cylinders in tandem: time histories of lift and drag coefficients of both upstream (subscript 1) and downstream (subscript 2) cylinders at $U^* = 4.2$ (left column) and $U^* = 6$ (right column).

$U^* = 6$ lies within the synchronization regime and, therefore, steady periodic oscillations are observed. On the other hand, beats are observed at $U^* = 4.2$. The lift force experienced by both cylinders are small at $U^* = 6$ compared to that at $U^* = 4.2$. This can also be seen from Fig. 9(a).

5.4. Hysteresis

Hysteresis in the response of a single cylinder at high Re, beyond the laminar regime, has been reported by many researchers in the past (Bishop and Hassan, 1964; Feng, 1968; Brika and Laneville, 1993; Khalak and Williamson, 1999). It is generally attributed to drastic change in the vortex shedding pattern. Singh and Mittal (2005) reported hysteresis in free vibrations in the laminar regime. They observed that the response of the cylinder is hysteretic at both ends of the lock-in regime. Prasanth et al. (2006) found that the hysteretic behaviour of the response of the cylinder at the lower Re end of lock-in depends on blockage. At lower blockage, the hysteretic behaviour of the cylinder is replaced by an intermittent switching of modes. The hysteretic behaviour at the higher Re end of lock-in, on the other hand, is not affected by blockage.

There have been very few studies for flow past a pair of cylinders undergoing free vibrations that considered hysteresis. Laneville and Brika (1999), in their experimental study of vortex-induced vibration of two flexible cylinders in tandem arrangement, reported hysteresis in the response of both cylinders. In the present study very low blockage is used ($B = 2\%$). As in the single cylinder results reported by Prasanth et al. (2006), the onset of lock-in at low U^* is not hysteretic for the upstream cylinder. The response of both the cylinders is found to be hysteretic in only two regions for the entire U^* range studied (Fig. 12). The first hysteretic loop is observed at $U^* \sim 7.0$ while the second one is at $U^* \sim 8.1$. The first hysteretic loop takes place close to U^* where the phase between the lift and transverse response of each of the two cylinders suffers a jump from 0° to 180°, approximately. The second hysteresis, as was observed for a single cylinder, takes place close to the higher U^* end of the synchronization range. The time histories of lift and drag coefficients along with the response of the cylinder for the fully developed solution at $U^* = 8.2$ are shown in Fig. 13 for both the cylinders. The time histories for the increasing and decreasing

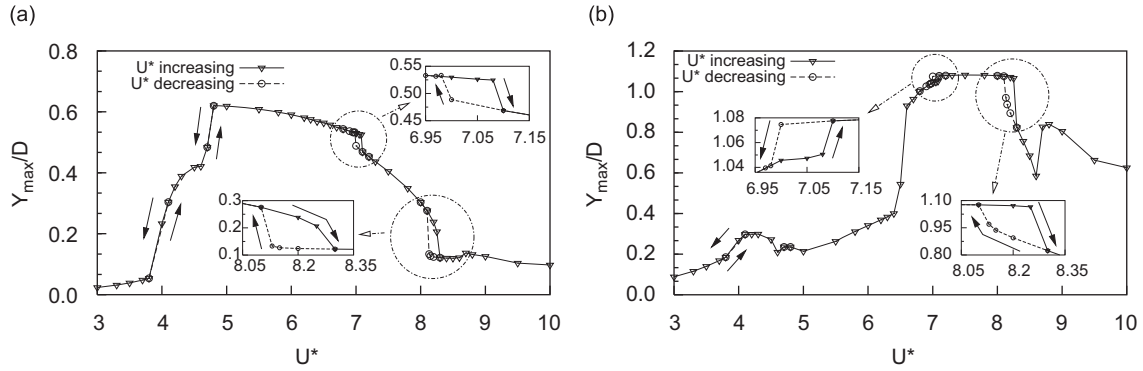

Fig. 12. Re = 100 flow past freely vibrating cylinders in tandem: variation of the transverse amplitude of oscillation of (a) upstream and (b) downstream cylinder with U^* for increasing and decreasing reduced speed.

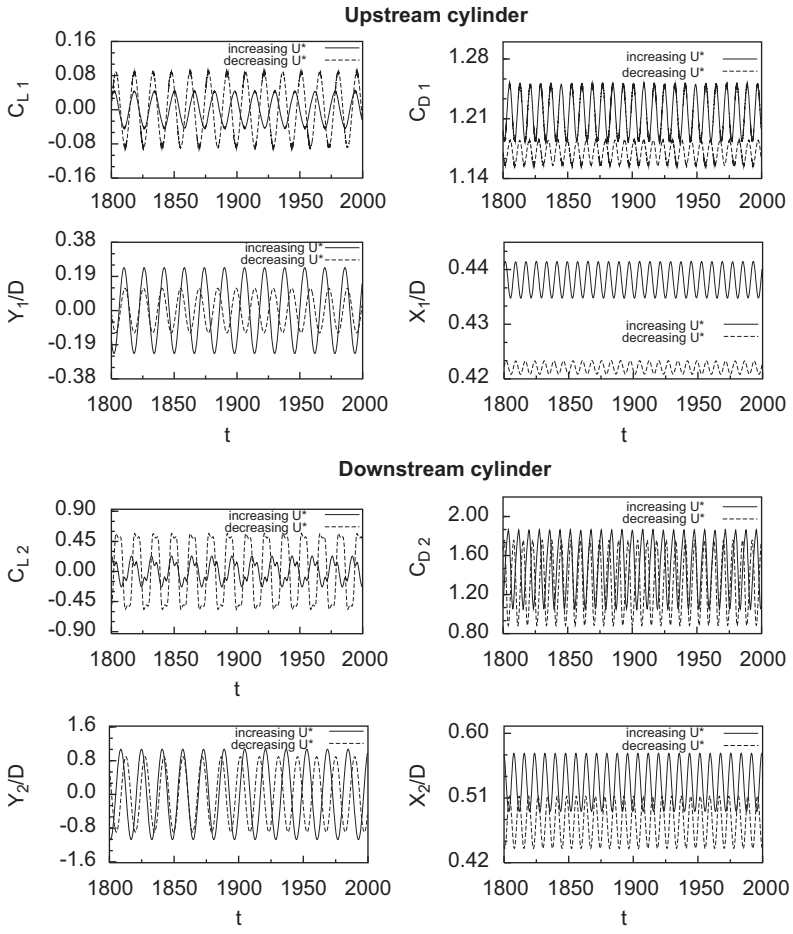

Fig. 13. Re = 100 flow past freely vibrating cylinders in tandem: time histories of lift and drag coefficients along with the response of the cylinders at $U^* = 8.2$ for both increasing and decreasing branches. Subscripts 1 and 2 denote the upstream and downstream cylinders, respectively.

U^* branches are found to be different for $U^* = 8.2$. This clearly shows the hysteretic behaviour at $U^* = 8.2$. A similar behaviour has also been observed at other values of U^* that lie within the hysteresis loop shown in the inset of Fig. 12.

5.5. The phase difference between lift and transverse displacement

Fig. 14 shows the variation of the phase difference, ϕ, between C_L and Y with U^*. The phase difference for both the upstream and downstream cylinders is shown in the figure, along with the variation of amplitude of transverse vibration of the cylinders. The phase difference, ϕ has been computed by using the Hilbert transform on the time histories for the lift force and displacement and was found to remain constant for a given reduced velocity. A similar study for the single cylinder case is reported in Prasanth and Mittal (2008), and details about the technique can be found in Khalak and Williamson (1999). In the present case, it is found that the lift and transverse oscillation of the cylinder are almost in phase until a jump of $\sim 180^\circ$ occurs at $U^* \sim 7.2$. The point of jump is same for both the cylinders and coincides with the point where the vortex shedding frequency matches the natural frequency of the system (Fig. 3). We have observed that for a certain range of U^* in which the maximum amplitude of oscillations undergoes sudden variation, the time histories of the lift for the downstream cylinder did not exhibit a very periodic behaviour. Consequently, the phase difference for these values of U^* showed significant variation with time. For example, for $8 \leqslant U^* \leqslant 9.5$ the phase difference for the downstream cylinder was not constant in time and is not shown in Fig. 14.

5.6. A possible explanation for the phase jump

Fig. 15 shows the time variation of the lift coefficient for a cycle of transverse oscillation of the cylinders for certain values of U^* before and after the phase jump. It is found that the power spectra of the lift coefficient shows an additional frequency: $\sim$3St (three times the Strouhal frequency) at U^*'s near the jump. This can be clearly seen from Fig. 16. At U^* very close to the jump, ($U^* = 7.5$, Fig. 15(b)), the component of lift coefficient corresponding to 3 St is more dominant than the one at St. However, if U^* is further increase in beyond the jump this component again becomes weak compared to the one at St.

In order to investigate further, the total lift coefficient, C_{LT} was decomposed into two parts: the viscous contribution, C_{LV} and pressure contribution, C_{LP}. Fig. 15 shows the pressure and viscous components along with the total lift coefficient for a cycle of cylinder oscillation for the upstream (left column) and downstream cylinders (right column). The cylinder response, Y/D is also shown. The variation of the components of lift coefficient is shown at three values of U^*: (a) $U^* = 6$, before the phase jump, (b) $U^* = 7.5$, just at the point of jump and (c) $U^* = 8.1$, after the phase jump. For all U^*, the viscous component of lift appears to maintain its phase with the cylinder motion for both upstream and downstream cylinders. However, the pressure component shows a contribution at frequency 3 St and a phase jump at $U^* = 7.5$. At $U^* = 8.1$, the pressure component is almost out of phase with the cylinder motion for both cylinders.

To analyse this change in phase of the pressure component of the lift, the C_p distribution on the cylinder surface for both the cylinders is plotted in Fig. 17 at a time instant when the cylinders are at their peak transverse displacement. The pressure variation on the cylinder surface can be divided into three regions: the regions near the front stagnation point with high C_p, the top and the bottom of the cylinder with low C_p as reported in Stewart et al. (2005) and Prasanth and Mittal (2008). The appearance of the phase shift in C_p is primarily caused by the change in the location of these three pressure regions along the cylinder surface and their relative values. This is very clear from the variation of C_p on

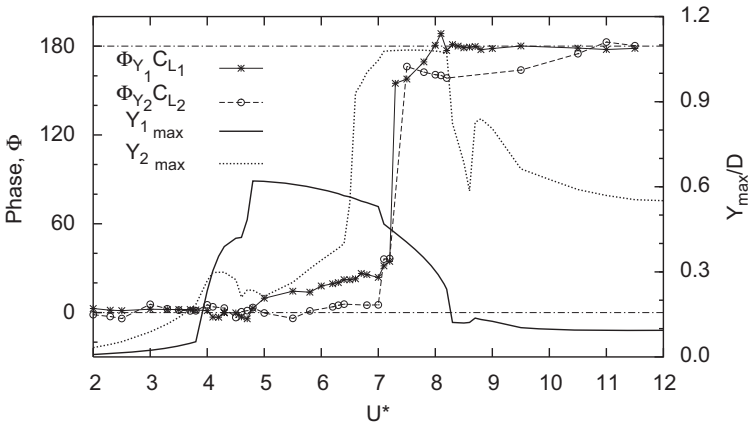

Fig. 14. Re = 100 flow past freely vibrating cylinders in tandem: variation of the phase difference between lift force and transverse displacement with U^*. For reference, the variation of the maximum transverse oscillation amplitude of the two cylinders is also shown.

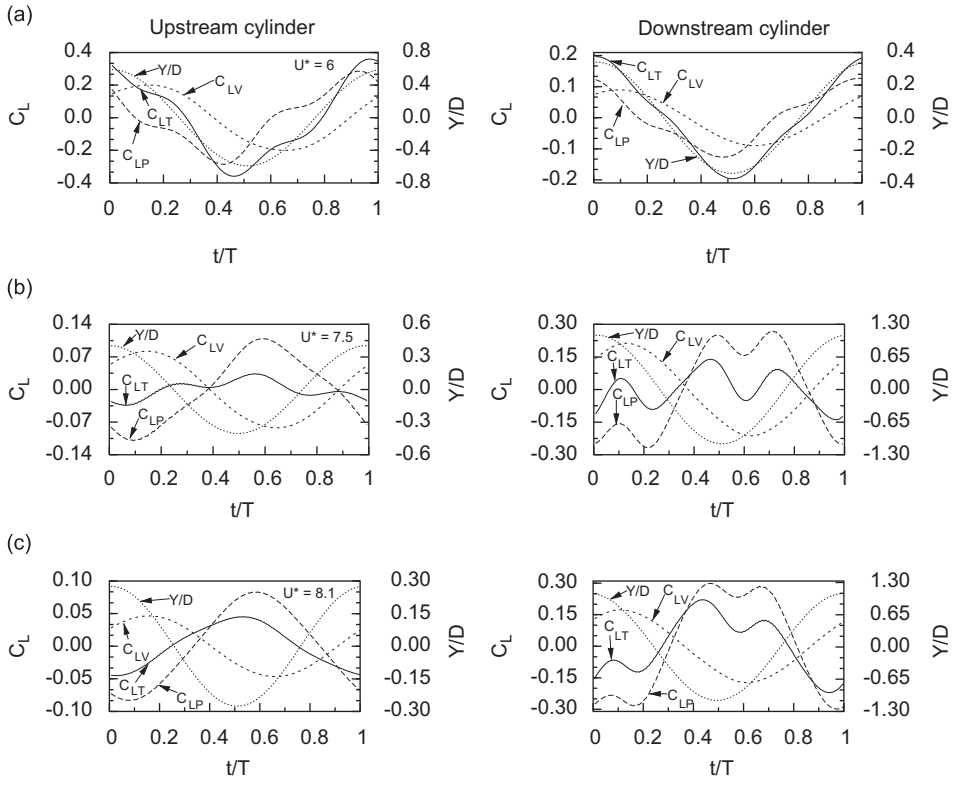

Fig. 15. Re = 100 flow past freely vibrating cylinders in tandem: time variation of the contributions of the pressure, C_{LP}, and viscous part, C_{LV}, to the total lift coefficient, C_{LT} during one cycle of transverse motion of the cylinders at (a) $U^* = 6$, (b) $U^* = 7.5$ and (c) $U^* = 8.1$. The transverse motion of the cylinders is also shown along with. The left column shows the variation for upstream cylinder and the right column shows the variation for downstream cylinder.

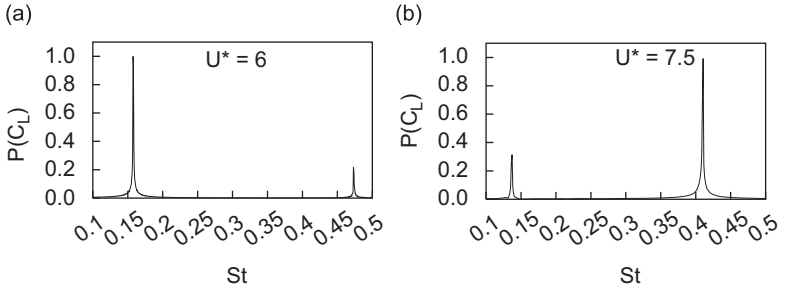

Fig. 16. Re = 100 flow past freely vibrating cylinders in tandem: power spectra of the time histories of lift coefficient for the upstream cylinder at (a) $U^* = 6.0$ and (b) $U^* = 7.5$.

the downstream cylinder surface. The variation of C_p on the upstream cylinder surface is similar to that observed for a single cylinder in Prasanth and Mittal (2008). For the upstream cylinder, it can be seen from Fig. 17(a) that the locations of the stagnation point and the maximum suction on the upper surface of the cylinder are the same for all U^* shown. However, the location of the maximum suction on the lower surface of the upstream cylinder is quite different for the three values of U^*. The suction at the upper surface for $U^* = 6$ is large compared to that on the lower surface. Consequently, the lift is upwards, leading to $\phi \sim 0$. At $U^* = 8.1$ the magnitude of peak suction at the upper and lower surfaces is comparable. However, on the lower surface it occurs at an angle of $\sim 85^\circ$ from the front stagnation point, and the overall C_p on the lower surface is fairly low. This results in an overall negative value of C_{LP} for $U^* = 8.1$ while

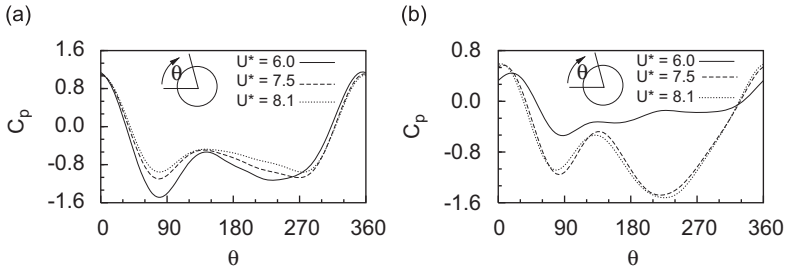

Fig. 17. Re = 100 flow past freely vibrating cylinders in tandem: variation of pressure coefficient on the surface of the cylinder at different U^* at the instant of maximum displacement of the cylinder for (a) upstream cylinder and (b) downstream cylinder.

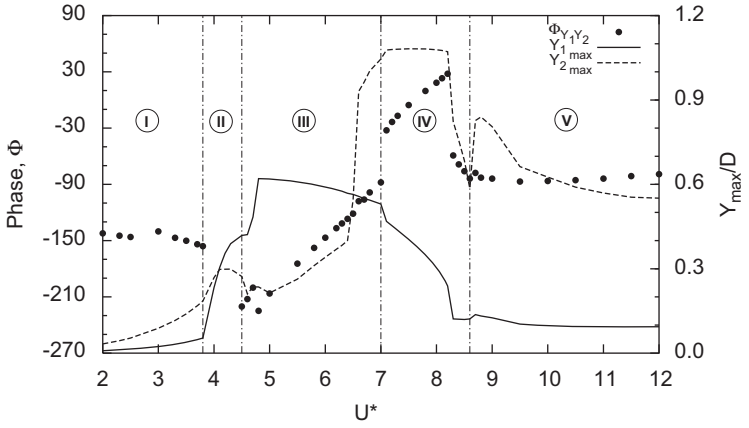

Fig. 18. Re = 100 flow past freely vibrating cylinders in tandem: variation of the phase difference between the transverse oscillations of the upstream and downstream cylinders with U^*. For reference, the variation of the maximum transverse oscillation amplitude of the two cylinders is also shown. The subscripts 1 and 2 denote the upstream and downstream cylinders, respectively.

it is positive at $U^* = 6$. This in turn causes the total lift force, C_{LT} to go out of phase with cylinder motion at $U^* = 8.1$. The downstream cylinder also shows a similar behaviour as can be seen from Figs. 15 and 17.

5.7. The phase difference between the transverse oscillations of upstream and downstream cylinders and vortex shedding modes

Fig. 18 shows the variation of phase difference between the transverse oscillations of the upstream and downstream cylinders, $\phi_{Y_1Y_2}$ with U^*. The variation of transverse displacement of both cylinders is also shown in the figure. It is seen that $\phi_{Y_1Y_2}$ undergoes large changes, and these changes correspond to the variation in the oscillation amplitude of both cylinders. Instantaneous vorticity fields for the fully developed unsteady flow, at various values of U^* are shown in Fig. 19. Based on the variation of $\phi_{Y_1Y_2}$ and the flow field with U^* we can classify the entire U^* regime into five sub-regions, as shown in Fig. 18.

Region I: For $U^* \leqslant 3.8$ the two cylinders oscillate with very small amplitudes and almost out of phase with each other ($\phi_{Y_1Y_2} \sim 150^\circ$). The vortex shedding frequency from the two cylinders is almost constant and the vortices coalesce just downstream of the second cylinder (Figs. 19(a,b)).

Region II: For $3.8 < U^* \leqslant 4.5$ the phase difference shows rapid time variations. This region includes the onset of synchronization, when the oscillation amplitude of both cylinders increases significantly. The transverse oscillation amplitude of the upstream cylinder is larger than that of the downstream one. Although the phase is quite irregular in this region, in general, during its upward motion the downstream cylinder comes in the way of a clockwise rotating vortex shed from the upper surface of the upstream cylinder. Similarly, in the downward motion, it encounters an anticlockwise rotating vortex shed from the lower surface of the upstream cylinder (Fig. 19(c)).

Region III: For $4.5 < U^* \leqslant 7$, $\phi_{Y_1Y_2}$ varies linearly with U^*. In this region both cylinders are in lock-in state. Merging of vortices takes place immediately downstream of the second cylinder to form a row of vortices. The far wake exhibits

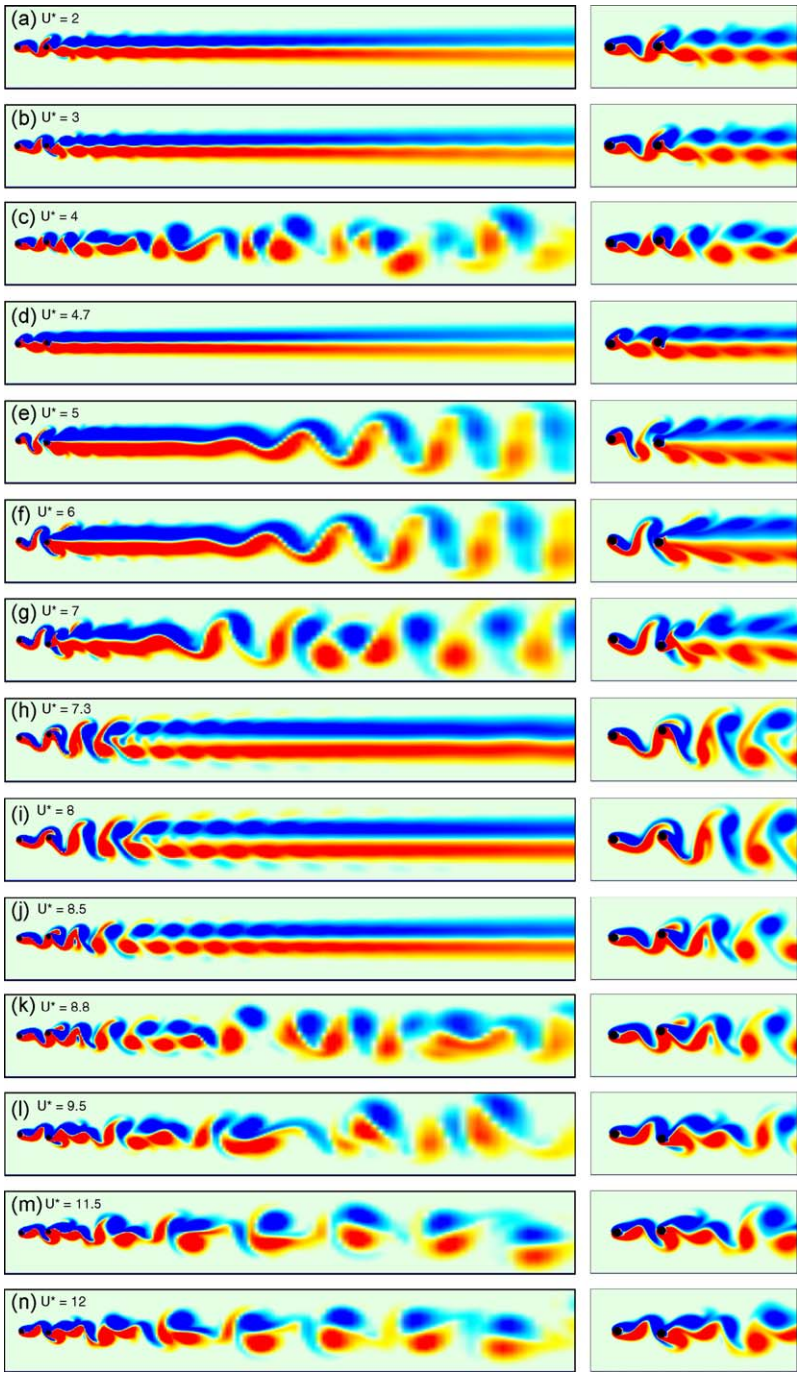

Fig. 19. Re = 100 flow past freely vibrating cylinders in tandem: instantaneous vorticity field for the fully developed unsteady flow at various reduced velocity, U^*. The right column shows close-up view of the flow near the two cylinders.

a low frequency secondary shedding (Figs. 19(e–g)). The point of onset of secondary shedding is found to move upstream with increase in U^*. The counter-clockwise rotating vortices that are shed from the lower surface of the upstream cylinder hit the downstream cylinder and each one splits into two. The one that glides along the upper surface gets diffused, while the one that moves towards the lower surface of the downstream cylinder interacts with the counter-clockwise rotating vortex shed from the second cylinder and produces a stronger vortex. The clockwise rotating vortices

shed from the upper side of the cylinders also undergoes a similar interaction and two rows of such vortices are seen in the wake downstream of the second cylinder.

Region IV: This regime ($7.1 \leqslant U^* \leqslant 8.6$) begins with a jump in the phase difference both between the transverse force and displacement and between the displacements of the upstream and downstream cylinders, $\phi_{Y_1 Y_2}$. A linear variation in the phase difference from $\sim -30^\circ$ to $+30^\circ$ is observed in this region. The downstream cylinder undergoes very large amplitude of oscillation in this range of U^*. For the most of this sub-region, the upstream cylinder is in lock-in state. Therefore, the vortex shedding frequency decreases with increase in U^*. For $U^* \sim 8.6$ the distance between the longitudinal vortices becomes large, almost equal to the separation between the cylinders. The vorticity plots for this regime are shown in Figs. 19(h–j). When the downstream cylinder is at its peak transverse location, a counter-clockwise rotating vortex, released from the lower surface of the upstream cylinder, is located just below the lower surface of the downstream cylinder. Compared to an isolated cylinder, this causes an increase in the suction on the lower surface of the downstream cylinder, thereby leading to larger amplitude oscillations. The strong vortices shed from the downstream cylinder coalesce in the wake giving rise to C(2S) type of shedding pattern. This is similar to the vortex shedding mode for large amplitude oscillations of a single cylinder reported by Singh and Mittal (2005) and Prasanth et al. (2006). Towards the end of this regime the cylinders go again out of phase. This is marked by a decrease in the oscillation amplitude for both cylinders. In order to check the role of numerical diffusion on the vorticity field in the far wake, computations for $U^* = 8$ were carried out on a more refined finite element mesh with 61 195 nodes. The refinement of the mesh is in the far wake region. The results from the refined mesh are virtually the same as obtained with the original mesh. This confirms that the coalescence of vortices in the far wake is a physical phenomenon.

Region V: For $U^* > 8.6$ the cylinders are beyond the state of lock-in. The upstream cylinder exhibits very low amplitude oscillations. The phase difference, $\phi_{Y_1 Y_2}$, remains almost constant at $\sim 90^\circ$. A regular *2S* mode of shedding, as defined in Williamson and Roshko (1988), is observed close to the upstream cylinder. However, the flow structure in the wake downstream of the second cylinder is very irregular and complex (Figs. 19(k–n)). For $U^* > 11$ the vortices in the far wake appear to organize themselves in well ordered pairs.

6. Summary

Results have been presented for the free vibrations of a pair of equal-sized circular cylinders of low nondimensional mass ($m^* = 10$) in tandem arrangement. The computations are carried out for various values of reduced speed ($2 < U^* < 15$). The Reynolds number, based on the free-stream speed and the diameter of the cylinders, is 100. A stabilized finite element method is utilized to carry out the computations in two dimensions. The response of the two cylinder system in tandem arrangement is compared with that of a single cylinder. It is found that, even though the transverse response of the upstream cylinder is qualitatively similar to that of a single cylinder, the presence of a downstream cylinder affects the upstream cylinder significantly. Compared to a single cylinder, the upstream cylinder undergoes synchronization at a lower U^*. Also, during lock-in the vortex shedding frequency is farther away from the natural frequency, compared to an isolated freely vibrating cylinder.

The downstream cylinder undergoes very large amplitude of oscillations in both transverse and streamwise directions. The peak amplitude of transverse oscillations is $1.1D$, approximately. This is almost twice the value observed for a single cylinder in laminar regime. The response of the downstream cylinder, with U^*, resembles that of a single cylinder at higher Re beyond the laminar regime. The upper branch, which does not exist for VIV of single cylinder in the laminar regime but is seen at larger Re, seems to be present for the downstream cylinder even in the laminar regime. The variation of the streamwise oscillations with U^* shows several local peaks at sub- and super-harmonic frequencies as well as at the boundaries of lock-in.

Lock-in/synchronization is observed for, both, upstream and downstream cylinders. The upstream cylinder undergoes lock-in at a lower U^* than the downstream one. Except at the onset, the frequency of vibrations of both the cylinders is identical for the entire U^* range. As is seen for a single cylinder, the phase difference between transverse response and lift force for both the cylinders goes through a $\sim 180^\circ$ jump in the middle of the synchronization regime. The jump occurs precisely at that value of U^* where the nondimensional frequency ratio, $f^* = f/f_N$ achieves the value 1.0. The phase jump is caused due to the size and relocation of suction peaks on the surface of the cylinders. The phase difference between the transverse oscillation of both cylinders is found to have a constant value outside the lock-in region. Inside the lock-in region, the phase difference is found to increase almost linearly with a jump in between at U^* where the downstream cylinder gets locked-in. The response of both the cylinders is hysteretic for two small regions of U^*. Depending on the phase between the transverse response of the two cylinders and the flow pattern, the entire flow regime is sub-divided into five regions.

Acknowledgement

Partial support for this work from the Department of Science and Technology, India is gratefully acknowledged.

References

Assi, G.R.S., Meneghini, J.R., Aranha, J.A.P., Bearman, P.W., Casaprima, E., 2006. Experimental investigation of flow-induced vibration interference between two circular cylinders. Journal of Fluids and Structures 22, 819–827.

Bearman, P.W., 1984. Vortex shedding from oscillating bluff bodies. Annual Review of Fluid Mechanics 16, 195–222.

Bishop, R.E.D., Hassan, A.Y., 1964. The lift and drag forces on a circular cylinder oscillating in a flowing fluid. Proceedings of Royal Society London, Series A 277, 51–75.

Bokaian, A., Geoola, F., 1984a. Wake-induced galloping of two interfering circular cylinders. Journal of Fluid Mechanics 146, 383–415.

Bokaian, A., Geoola, F., 1984b. Proximity-induced galloping of two interfering circular cylinders. Journal of Fluid Mechanics 146, 417–449.

Brika, D., Laneville, A., 1993. Vortex induced vibrations of long flexible circular cylinder. Journal of Fluid Mechanics 250, 481–508.

Carmo, B.S., Sherwin, S.J., Bearman, P.W., Willden, R.H.J., 2007. Numerical simulation of the flow-induced vibration in the flow around two circular cylinders in tandem arrangements. In: Fifth Conference on Bluff Body Wakes and Vortex-induced Vibrations, Costa do Sauipe, Brazil.

Feng, C.C., 1968. The measurement of vortex-induced effects in flow past a stationary and oscillating circular cylinder and D-section cylinders. Master's Thesis, University of British Columbia, Vancouver, Canada.

Jester, W., Kallinderis, Y., 2004. Numerical study of incompressible flow about transversely oscillating cylinder pairs. ASME Journal of Offshore Mechanics and Arctic Engineering 126, 310–317.

Khalak, A., Williamson, C.H.K., 1999. Motion, forces and mode transitions in vortex-induced vibrations at low mass damping. Journal of Fluids and Structures 13, 813–851.

King, R., Johns, D.J., 1976. Wake interaction experiments with two flexible circular cylinders in flowing water. Journal of Sound and Vibration 45, 259–283.

Laneville, A., Brika, D., 1999. The fluid and mechanical coupling between two circular cylinders in tandem arrangement. Journal of Fluids and Structures 13, 967–986.

Mahir, N., Rockwell, D., 1996a. Vortex formation from a forced system of two cylinders, part 1: tandem arrangement. Journal of Fluids and Structures 10, 473–489.

Mahir, N., Rockwell, D., 1996b. Vortex formation from a forced system of two cylinders, part 2: side-by-side arrangement. Journal of Fluids and Structures 10, 491–500.

Mittal, S., 1992. Stabilized space-time finite element formulation for unsteady incompressible flows involving fluid-body interaction. Ph.D. Thesis, University of Minnesota, USA.

Mittal, S., Singh, S.P., Kumar, B., Kumar, R., 2006. Flow past bluff bodies: effect of blockage. International Journal of Computational Fluid Dynamics 20, 163–173.

Mittal, S., Kumar, V., Raghuvanshi, A., 1997. Unsteady incompressible flow past two cylinders in tandem and staggered arrangements. International Journal of Numerical Methods in Fluids 25, 1315–1344.

Mittal, S., Kumar, V., 1999. Finite element study of vortex-induced cross-flow and in-line oscillations of a circular cylinder at low Reynolds numbers. International Journal of Numerical Methods in Fluids 31, 1087–1120.

Mittal, S., Kumar, V., 2001. Flow-induced oscillations of two cylinders in tandem and staggered arrangement. Journal of Fluids and Structures 15, 717–736.

Mittal, S., Kumar, V., 2004. Vortex-induced vibrations of a pair of cylinders at Reynolds number 1000. International Journal of Computational Fluid Dynamics 18, 601–614.

Mittal, S., Tezduyar, T.E., 1992. A finite element study of incompressible flows past a oscillating cylinders and airfoils. International Journal for Numerical Methods in Fluids 15, 1073–1118.

Papaioannou, G.V., Yue, D.K.P., Triantafyllou, M.S., Karniadakis, G.E., 2006. Three-dimensionality effects in flow around two tandem cylinders. Journal of Fluid Mechanics 558, 387–413.

Papaioannou, G.V., Yue, D.K.P., Triantafyllou, M.S., Karniadakis, G.E., 2008. On the effect of spacing on the vortex-induced vibrations of two tandem cylinders. Journal of Fluids and Structures 24, 833–854.

Prasanth, T.K., Behara, S., Singh, S.P., Kumar, R., Mittal, S., 2006. Effect of blockage on vortex-induced vibrations at low Reynolds numbers. Journal of Fluids and Structures 22, 865–876.

Prasanth, T.K., Mittal, S., 2008. Vortex-induced vibrations of a circular cylinder at low Reynolds numbers. Journal of Fluid Mechanics 594, 463–491.

Sarpkaya, T., 2004. A critical review of the intrinsic nature of vortex-induced vibrations. Journal of Fluids and Structures 19, 389–447.

Singh, S.P., Mittal, S., 2005. Vortex-induced oscillations at low Reynolds numbers: hysteresis and vortex shedding modes. Journal of Fluids and Structures 20, 1085–1104.

Stewart, B.E., Leontini, J.S., Hourigan, K., Thompson, M.C., 2005. A numerical study of wake modes and energy transfers for an oscillating cylinder at $Re = 200$. In: Fourth Symposium on Bluff Body Wakes and Vortex-Induced Vibrations, Greece.

Sumner, D., Price, S.J., Paidoussis, M.P., 2000. Flow pattern identification for two staggered circular cylinders in cross flow. Journal of Fluid Mechanics 411, 263–303.

Tezduyar, T.E., Behr, M., Liou, J., 1992a. A new strategy for finite element computations involving moving boundaries and interfaces—the deforming-spatial-domain/space-time procedure I: the concept and the preliminary tests. Computer Methods in Applied Mechanics and Engineering 94, 339–351.

Tezduyar, T.E., Behr, M., Mittal, S., Liou, J., 1992b. A new strategy for finite element computations involving moving boundaries and interfaces- the deforming-spatial-domain/space-time procedure, II: computations of free-surface flows, two liquid flows and flows with drifting cylinders. Computer Methods in Applied Mechanics and Engineering 94, 353–371.

Tezduyar, T.E., Mittal, S., Ray, S.E., Shih, R., 1992c. Incompressible flow computations with stabilized bilinear and linear equal-order-interpolation velocity pressure elements. Computer Methods in Applied Mechanics and Engineering 95, 221–242.

Williamson, C.H.K., Govardhan, R., 2004. Vortex induced vibration. Annual Review of Fluid Mechanics 36, 413–455.

Williamson, C.H.K., Roshko, A., 1988. Vortex formation in the wake of an oscillating cylinder. Journal of Fluids and Structures 2, 355–381.

Zdravkovich, M.M., 1977. Review of flow interference between two circular cylinders in various arrangements. ASME Journal of Fluids Engineering 99, 618–633.

Zdravkovich, M.M., 1985. Flow-induced oscillations of two interfering circular cylinders. Journal of Sound and Vibration 101, 511–521.